Impact of hydrate saturation on water permeability in hydrate-bearing sediments

[1]Nariman Mahabadi, [2]Sheng Dai, [3]Yongkoo Seol, and [4]Jaewon Jang

[1]School of Sustainable Engineering and the Built Environment, Arizona State University, USA
[2]School of Civil and Environmental Engineering, Georgia Institute of Technology, USA
[3]National Energy Technology Laboratory, USA
[4]Department of Civil and Environmental Engineering, Hanyang University, Korea
Corresponding author, email: jwj@hanyang.ac.kr

Abstract: 211 words
Text: 3031 words (not including abstract, references and figure captions)
Table: 1
Figure: 5

Keywords: water permeability, hydrate-bearing sediments, hydrate saturation, wave velocity, pore network model, pore habit

Index terms: 3004 gas and hydrate systems; 3022 marine sediments: processes and transport

Abstract

Permeability of the hydrate-bearing sediments critically affects the hydrate dissociation process as well as the rate and efficiency of gas production. Reported permeability values are observed to be widely are very scattered owing to the dependence on multiple factors such as experimental conditions and test procedures. It is critical that the permeability is measured accurately to enable prediction of long-term gas production using numerical simulation for an economic development of hydrate-bearing reservoirs. In this study, the tetrahydrofuran (THF) hydrates that exhibit pore habits of the pore-filling pattern are formed in sediments, and the water permeability is quantified as a function of hydrate saturation. The results show that a decrease in the permeability for an increase in the hydrate saturation. Based on the measured values that are bounded by Kozeny grain-coating and pore-filling models, the fitting parameters of the empirical permeability models are suggested for use in numerical simulation of long-term hydrate dissociation. Wave velocity measurements reveal pore habits of pore-filling pattern of THF hydrates in the sediments with S_h<0.5, and a gradual transition to patchy and load-bearing pore-habits when S_h>0.6. The numerical simulation results obtained using the complementary pore-network model suggest that the THF hydrates in the sediments may form in small clusters with an average patch size of ~4 pores.

1. Introduction

The permeability of the hydrate-bearing sediments is a governing factor to depressurization propagation and heat transfer associated with fluid flow during gas production from hydrate deposits. The permeability can be incorporated into numerical simulations to predict the long-term hydrate dissociation for an economic development of a hydrate-bearing reservoir. In clayey sediments that exhibit a low permeability, the hydrate dissociation via depressurization occurs at a very narrow interface (i.e, short dissociation front) between the free gas zone and the hydrate-bearing zone. However, in sandy sediments that exhibit a high permeability, the hydrate dissociation occurs over a wider interface [1-3].

Hydrate saturation and hydrate pore habit are known to be the important characteristics governing the permeability and water retention characteristics [4-7]. The permeability may vary with the hydrate pore habit by a few orders of magnitude even at the same hydrate saturation [8, 9]. The pore habit of the natural hydrate-bearing sediments is found to be of pore-filling pattern based on the in-situ seismic analysis for the Blake Ridge [10] and the Mallik sites [11, 12], and the wave velocity measurements on the pressure cores recovered from the Nankai Trough [13]. However, most laboratory-formed hydrate-bearing sediments exhibit pore habits of grain-coating or contact-cementing pattern if formed in an unsaturated condition, i.e., using the excess-gas method [14]. This method is generally preferred to be employed in the laboratory owing to its reduced time of hydrate formation (Table 1). The measured values of permeability of the laboratory-formed hydrate-bearing sediments may not represent those of the in-situ (natural) hydrate-bearing sediments properly, because of the difference in pore habits; therefore, the applicability of the published values of permeability (laboratory tested values) to in-situ gas production needs to be reexamined [15]. It is evident from Figure 1 that the permeability data resulted from various experimental methods, specimen types, and testing conditions are widely scattered.

The pore habit of the tetrahydrofuran (THF) hydrates formed in the sediments under a saturated conditions is of pore-filling pattern, which has been confirmed by seismic measurement [16], X-ray computed micro-tomography [17, 18], and direct visualization through transparent microfluidic chips [4]. Built upon a comprehensive review of previous studies on permeability in hydrate-bearing sediments, this study measures for the first time the permeability of sediments

containing various saturation of THF hydrate. Corresponding P- and S-wave velocities are also monitored to identify the effect of the hydrate on sediments stiffness and the effect of water flow on hydrate saturation during the permeability tests. Moreover, simulation is performed using pore-network model to investigate the effect of the hydrate patch size on permeability.

2. Permeability models and experimental data

Permeability models. The analytical models for water permeability, k_{rw}, as a function of hydrate saturation, S_h, developed considering the shape of the pore space (e.g., capillary tube model and Kozeny grain model) and the location of hydrates in the pore space (e.g., surface coating and pore-filling), are represented by the following Equations 1~4 [6, 19].

Capillary tube	Grain-coating	$k_{rw}=(1-S_h)^2$	(1)
	Pore-filling	$k_{rw}=1-S_h^2+2(1-S_h)^2/\log(S_h)$	(2)
Kozeny grain	Grain-coating	$k_{rw}=(1-S_h)^{n+1}$	(3)
		where $n=1.5$ for $0<S_h<0.8$ and $n>1$ for $S_h>0.8$	
	Pore-filling	$k_{rw}= (1-S_h)^{n+2}/(1+S_h^{0.5})^2$	(4)
		where $n=0.7S_h+0.3$	

The permeability calculated by the capillary tube and Kozeny grain models are shown in Figure 1. The capillary tube model provides a wider range of the values of permeability values at a given hydrate saturation compared to the Kozeny grain model.

Permeability data. The values of permeability measured in the laboratory-formed and natural hydrate-bearing sediments have been compiled from the literature (Figure 1). As shown in Table 1, these measurements are obtained under various experimental conditions: different gases (CH_4 or CO_2), hydrate formation methods (excess-gas, excess-water, ice-seeding, or gas-bubbling), permeability measurement methods (water flow, gas flow, nuclear magnetic resonance, or well-logging), sediment types and dimensions (artificially formed hydrate-bearing sediments, conventional and pressure cores recovered from hydrate reservoirs).

The majority of the laboratory studies published in the literature have employed the excess-gas method in order to expedite the hydrate formation in sediments. However, this method exhibits several limitations as follows:

- Hydrate pore habits. The pore habit of the hydrates formed under un unsaturated condition (excess-gas or water-limited condition) may not represent the pore habit of the hydrates in natural sediments with a saturated condition; thus, the excess-gas method exhibits a discrepancy in permeability with reference to the natural sediments.
- Specimen saturation. The excess-gas method generates unsaturated specimens, which need to be saturated for permeability measurement. However, saturating the specimens is a challenging task due to the trapped gas bubbles as well as the possibilities of dissociation and additional formation of hydrates.
- Hydrate dissolution. If pure water is circulated for permeability measurement, the hydrates can dissolve even under a hydrate-stable pressure-temperature condition owing to the solubility of gas in water with the existence of hydrates [20]. As a result, the water permeability may increase gradually with time [21]. On the other hand, the injection of a stream of gas-saturated water can induce formation of additional hydrates because of the difference in the values of gas solubility with and without the existence of hydrates [22-24].
- Hydrate formation. Initially, hydrates form at the water-gas interfaces, and the formed hydrate films slow down the mass transfer that is essential to sustain further hydrate formation. Therefore, the conversion ratio, i.e., the ratio of the amount of water reacted to form the hydrates over the initial amount of water, hardly ever reaches 100% within the limited period of the experiment [25]. This conversion ratio decreases as the initial water saturation increases [8].

As shown in Figure 1, some experimental values of permeability are much lower than the range predicted by the permeability models. In fact, the values are even lower than those predicted by the pore-filling model, which predicts the lowest values among other analytical models. A few possibilities for the low permeability values are listed as follows:

- For the excess-gas method, the hydrates form at the gas-water interface. The water that is not used to form the hydrates remains immobile below the hydrate layer thereby not

contributing to the permeability [8, 26, 27]. Therefore, the method results in a lower permeability compared to the other hydrate pore habits at a given water saturation.

- Initially, the water is distributed only at the grain contacts, and therefore, the hydrates form predominantly at the pore throats, thereby plugging the path of water flow. Therefore, the measured values of permeability can be very low even at low hydrate saturation.
- If pure water is injected during the measurement of permeability, gas bubbles are generated due to hydrate dissolution. These gas bubbles may then get trapped in the pore space, thereby lowering the value of permeability [21].
- Permeability is measured at different levels of hydrate saturation by nuclear magnetic resonance (NMR) technique while the hydrates dissociate from S_h=0.33 to lower S_h [23]. The gas bubbles evolved during this process can get trapped, thereby lowering the value of permeability.

3. Experimental Details

A falling head permeameter cell (Humboldt Mfg. Co., Model: HM-5982) was modified to measure the permeability as a function of hydrate saturation (Figure 2a). The original acrylic cylinder (15.2 cm in height and 8.9 cm in diameter) of the cell was replaced with an aluminum cylinder of the same dimensions [28]. The piezo-crystals (APC International, Ltd., MFT-15T-6.7A1 RoHS) and bender elements (Piezo Systems, T2LCH) were installed in the cylinder for P- and S-wave velocity measurements. A function generator (Agilent, 33210A), an oscilloscope (Keysight, DSOX-3014A), and a filter/amplifier (Krohn-Hite, model: 3364) were connected to the piezo-crystals and bender elements for velocity measurement (Figure 2b). The thermocouples (Conax Technologies, K-type) connected to the data-logger (Agilent, 34972A) were fitted to the cell to monitor the temperature profile during the hydrate formation and permeability measurement. The setup was placed in an environmental chamber for an accurate control of the temperature.

Three layers of sands (passing through #10 sieve and retained on #200 sieve, ASTM C778) were compacted into the cylinder (the porosity of the sediment is n=0.39). Two wire meshes were placed at the bottom and top of the sediments to prevent migration of sand grains during the permeability test. The water-THF solution was then injected into the compacted sediments in the mass ratios ranging from 92:8 (S_h=0.4) to 87:13 (S_h=0.7). It may be noted that the saturation of actually

formed THF hydrates is found to be lower than the THF hydrate saturation calculated by the mass ratio [30]. Then, the temperature was decreased to 0.5 ˚C to trigger the hydrate nucleation. The hydrate formation was indicated by the thermal peaks, and subsequently, the chamber was allowed to remain at the same temperature for 3 days to ensure complete conversion to THF hydrates. However, it was also ensured that the temperature and wave velocity attained stability without any further changes in their values. Subsequently, the valve of the water column was opened, followed by the falling head permeability test. The permeability measurement was performed three times at each of the identified levels of hydrate saturation. The P- and S-wave velocities were measured after each permeability test.

It must be mentioned that the permeability was not measured for hydrate saturation S_h<0.4 or S_h>0.7 because it was nearly infeasible to perform the test for practical reasons. For S_h lower than 0.4, the equilibrium temperature is at the most 0 °C (for water-excess condition). This low temperature may induce the water in the pores to freeze, thereby making the measurement infeasible. Mahabadi et al. (2016) has compiled the equilibrium temperatures of the THF hydrates as a function of water fraction in water-THF solution. The equilibrium temperatures of the other gas hydrates can be found in the references [31-33]. For S_h higher than S_h=0.7, the majority of the pore space is occupied by the hydrates, and thus shuts off the flow. This too causes the experimental measurement practically impossible.

4. Experimental Results and Analyses

Water permeability as a function of hydrate saturation. Water permeability experiments were performed on the sediments with hydrate saturation S_h=0, 0.4, 0.5, 0.6, and 0.7. The selected water-THF mass ratio results in the water as the only pore fluid after hydrate formation. The values of water permeability measured at each hydrate saturation were normalized by the water permeability at S_h=0. As shown in Figure 3a, the normalized permeability decreases as the hydrate saturation increases. The values of permeability are observed to be bounded by the Kozeny grain models. The permeability at S_h=0.4 lies between the predictions of the grain-coating model and the pore-filling model. Permeability becomes closer to the pore-filling model results as the hydrate saturation increases (S_h=0.6 and 0.7), which is consistent with previous experimental results [1, 34].

The permeability measurement was performed three times at a given hydrate saturation. The measured value increases slightly with the repetition of the test (Figure 3b). As shown in the inset of the Figure 3b, the 2nd and 3rd measurements show 3-7% increase compared to the 1st measurement. And the increase in measured permeability during the repeated tests is more pronounced in sediments with higher initial hydrate saturation, i.e., ~3% increase for S_h=0.4, and ~7% increase for S_h=0.7 condition.

The empirical models for permeability as a function of hydrate saturation, available in the published literature, include the University of Tokyo model (Equation 5) [35], a hybrid model (Equation 6) considering both grain-coating and pore-filling hydrate pore habits [34, 36], and a modified Corey model (Equation 7) [37]. In addition, equations based on the numerical simulation by Lattice Boltzmann method and pore-network modeling are also proposed considering the capillary effect and tortuosity (Equations 8 and 9) [9, 19]:

University of Tokyo model [35]

$k_{rw}=(1-S_h)^N$ N: permeability reduction exponent (5)

Hybrid model [34, 36]

$k_{rw}=\alpha k_{rw}^{pf}+\beta k_{rw}^{gc}$ (6)

where, $\alpha=S_h^L$, $\beta=(1-S_h)^M$, and k_{rw}^{pf} and k_{rw}^{gc} are the permeabilities calculated by Kozeny pore-filling and grain-coating models (Equations 3 and 4)

Modified Corey model [38]

$k_{rw}=(1-S_h)\cdot\exp(-C\cdot S_h)$ C: fitting parameter

(7)

Linear equation for capillary grain-coating [9]

$k_{rw}= -1.8\times S_h+1$ (8)

Modified Kozeny-Carman [19]

$k_{rw}=(1-S_h)^3/(1+2S_h)^2$ (9)

The empirical models (Equation 5-7) were fitted to the experimental values of permeability in order to get the fitting parameters. It must be mentioned here that only the values of the 1st measurement were used for fitting. The normalized mean square error (NMSE) [34, 36] was used

to estimate the differences between the measured permeability k_{rw}^{exp} and predicted permeability k_{rw}^{pre}.

$$\mathrm{NMSE} = \frac{1}{N}\left[\sum_1^N \left(k_{rw}^{exp} - k_{rw}^{pre}\right)^2\right] \Big/ \left[\left(\frac{1}{N}\sum_1^N k_{rw}^{exp}\right)\left(\frac{1}{N}\sum_1^N k_{rw}^{pre}\right)\right] \quad (10)$$

Based on the lowest NMSE, the fitting parameters for the abovementioned empirical models were obtained: N=3.22 for the University of Tokyo model, L=0.67 and M=1.30 for the hybrid model, and C=3.03 for the modified Corey model. Especially for the hybrid model, there were ranges of values for L and M that resulted in the values of permeability higher than 1, $k_{rw}>1$, for a certain range of hydrate saturation, while the combination of L and M parameters resulted in the lowest NMSE. Therefore, it was necessary to check the permeability values within the whole saturation range for the hybrid model. Accordingly, the permeability curves predicted by these empirical models using the identified fitting parameters were superimposed on the experimental results (Figure 3a).

Compressional and shear wave velocity. Compressional V_P and shear V_S wave velocities were measured for each condition of hydrate saturation prior to and immediately after the permeability test (Figure 4). The results show that V_P and V_S increase with hydrate saturation. Apart from the experiments, the P- and S-wave velocities were also computed for different hydrate pore habits using the rock physics models. Accordingly, the computational results were obtained for the contact-cementing, surface-coating, load-bearing, and pore-filling pore habits using the formulations in Dvorkin, Helgerud [39] and Mavko, Mukerji [40], and the results of the patchy model were obtained using the self-consistent model [41]. The experimental results are observed to follow the pore-filling pattern for $S_h<0.5$, while the data points lie between the predictions from the load-bearing model and the patchy model for $S_h>0.6$. For pore-filling hydrates, V_P and V_S do not show an evident increase until the hydrate saturation exceeds ~40% [42], which is consistent with our experimental results.

As shown in the insets in Figure 4, the P- and S-wave velocities decrease with the repetition of the permeability measurement, whereas the permeability increases (Figure 3). This implies that there exists a possibility of hydrate dissolution considering that pure water is injected [20, 21] and/ or

small hydrate particles are flushed out during the repeated permeability tests similar to the phenomenon of fines migration [43]. Volatilization of THF before the hydrate formation and incomplete conversion of the water-THF solution to THF hydrate may also result in a lower hydrate saturation compared to the target saturation level. In addition, during the permeability test, the drag force applied to hydrate particles may cause the hydrate particles to be flushed out of the sediment packing [44].

5. Pore-network model simulation – The effect of pore habit on permeability reduction

A pore-network model was used to investigate the effect of hydrate pore habit on permeability reduction curves. A detailed explanation of the pore-network model and simulation algorithm can be found in previous studies [5, 7, 45]. There could be a couple of issues in using the pore-network model such as the difference in capillary pressure between an irregularly shaped pore and a perfectly circular pore and the dependence of the interfacial tension on simulation pressure condition during the two-phase fluid simulation [46, 47]. In this simulation involving calculation of permeability, it is considered that the hydrates are solid phase, and only the liquid phase (water) occupies in the pore space (no gas phase is considered).

Initially, the hydrates were assigned to fill either a single pore (i.e., the distributed case) or a couple of neighboring pores (i.e., patchy formation). The number of pores in a patchy hydrate varies, e.g., 4, 64, or 1024 pores, as illustrated in Figure 5a. Following the distribution of the hydrates in the pores, the permeability was calculated using the hydrate-bearing pore-network model. The calculation was then performed for each hydrate saturation using 10 random realizations of the hydrate distribution with the same pattern in the pore network. The averaged values are plotted in Figure 5b for different sizes of the patch. It is evident that the permeability decreases as the hydrate saturation increases, the permeability of the distributed case is the lowest, and the permeability for the 1024-pore patch is the highest at a given hydrate saturation. This is because the individually distributed hydrate pores plug the water flow channels and thereby prevent formation of a global flow channel easily. However, if there is a big hydrate patch in the pore-network model, the water can freely flow through the other regions of the pore-network bypassing the hydrate patch. It is evident from Figure 5b that the experimental values of permeability lie close to the normalized curve of the 4-pore patch.

6. Conclusions

The permeability of the hydrate-bearing sediments is affected by hydrate saturation and hydrate pore habit. Hydrate formation (at unsaturated condition) in the laboratory using the excess-gas method results in grain-coating and/or contact-cementing pore habits that differ from the pore-filling hydrate pore habit observed in natural sediments. The experimental values of permeability compiled from the literature are observed to be widely scattered owing to the dependence on multiple factors such as the experimental conditions, sediment types, and test procedures. In this study, the THF hydrates known to have the pore-filling pore habit were formed in sands, and the permeability of the resultant hydrate-bearing sediments was measured. The results show that the measured values are bounded by the permeability curves of the Kozeny grain model, with the values lying closer to the pore-filling curve of the model as the hydrate saturation increases. The permeability is observed to increase with repeated measurements even when the hydrate saturation is held constant, which implies hydrate dissolution. This is also evidenced by the decreases in measured wave velocities. The empirical permeability models are fitted to the experimental results, and the fitting parameters are suggested. The wave velocity measurements in the THF hydrate-bearing sediments suggest a pore-filling pattern for $S_h<0.5$ and an intermediate pattern bounded by the patchy and load-bearing pore habits for $S_h>0.6$. The results of the simulations using the pore-network model imply that the THF hydrates may form in small clusters in the sediments with an average patch size of approximately 4 pores.

Acknowledgment

This work was supported by the research fund of the Korea Agency for Infrastructure Technology Advancement (18CTAP-C142849-01) and the National Energy Technology Laboratory (NETL) of US DOE. The authors greatly thank Dr. Timothy Kneafsey in Lawrence Berkeley National Laboratory for sharing his experimental data. The data presented in this study are available at http://jwjang1977.wixsite.com/mysite/data.

Table 1. Summary of permeability tests in hydrate-bearing sediments.

Type		Measure Method	Formation Method	Sediment	References
Artificially-Formed Hydrates	CH_4 Hydrate	CH_4 gas flow	Excess gas	N/A	Liang, Song [8]
			Ice seeding	Clayey	Liu, Wu [48]
			Ice thawing	Ksand / F110 / F110+Silt	Kneafsey, Seol [15]
				F110	Gupta [49]
		Water flow	Excess gas	Sands	Sakamoto, Komai [27] Sakamoto, Komai [26]
				Core recovered (Mt. Elbert)	Johnson, Patil [50]
				Toyoura sand No.7 & 8 sand Mallik simulated sand	Minagawa, Ohmura [21]
				Toyoura sand	Minagawa, Nishikawa [51]
		NMR/ Water flow	Excess gas (Gas bubbling)	Silica sand	Minagawa, Nishikawa [23] Minagawa, Nishikawa [24] Minagawa, Sakamoto [22]
			Excess gas/ Excess water	Silica sand	Minagawa, Egawa [52]
		NMR	Gas bubbling	Berea sandstone	Kleinberg, Flaum [6]
		PNM	Not described	Uniform-sized quartz	Wang, Zhao [53]
	CO_2 Hydrate	Water flow	Excess gas	Ottawa 20/30	Delli and Grozic [34]
				Silty fine sands	Liu, Zhang [54]
		CO_2 Gas flow	Excess gas	Glass beads	Kumar, Maini [1]
		Gas flushing		Sand + kaolin	Chuvilin and Grebenkin [55]
	R11	Liquid flow	Excess gas	Sand μ=280μm	Berge, jacobsen [56]
Naturally-Formed Hydrates	Pressurized core	NMR	In-situ	Silt (70%) and clay (15-30%)	Li, Zhao [57]
		Water flow		Nankai Trough (silty sand)	Santamarina, Dai [13]
					Priest, Druce [58]
					Konno, Yoneda [59]
		Consolidation			Yoneda, Masui [60]
	Well-logging	NMR		Mallik 5L-38	Lee [61]
					Kleinberg, Flaum [62]
				Nankai Trough	Murray, Fukuhara [63]

References

1. Kumar, A., B. Maini, P.R. Bishnoi, M. Clarke, O. Zatsepina, and S. Srinivasan, *Experimental determination of permeability in the presence of hydrates and its effect on the dissociation characteristics of gas hydrates in porous media.* Journal of Petroleum Science and Engineering, 2010. **70**(1-2): p. 114-122.

2. Jang, J. and J.C. Santamarina, *Hydrate bearing clayey sediments: Formation and gas production concepts.* Marine and Petroleum Geology, 2016. **77**: p. 235-246.

3. Santamarina, J.C. and J. Jang, *Gas production from hydrate bearing sediments: Geomechanical implicaitons.* Fire in the ice, 2009. **9**: p. 18-22.

4. Mahabadi, N., X. Zheng, and J. Jang, *The effect of hydrate saturation on water retention curves in hydrate-bearing sediments.* Geophysical Research Letters, 2016. **43**(9): p. 4279-4287.

5. Mahabadi, N. and J. Jang, *Relative water and gas permeability for gas production from hydrate-bearing sediments.* Geochemistry, Geophysics, Geosystems, 2014. **15**: p. 2346-53.

6. Kleinberg, R.L., C. Flaum, D.D. Griffin, P.G. Brewer, G.E. Malby, E.T. Peltzer, and J.P. Yesinowski, *Deep sea NMR: Methane hydrate growth habit in porous media and its relationship to hydraulic permeability, deposit accumulation, and submarine slope stability.* Journal of Geophysical Research, 2003. **108**(B10): p. 2508.

7. Mahabadi, N., S. Dai, Y. Seol, T.S. Yun, and J. Jang, *The water retention curve and relative permeability for gas production from hydrate-bearing sediments: pore-network model simulation.* Geochemistry, Geophysics, Geosystems, 2016. **17**: p. 3099-3110.

8. Liang, H., Y. Song, Y. Chen, and Y. Liu, *The measurement of permeability of porous media with methane hydrate.* Petroleum Science and Technology, 2011. **29**: p. 79-87.

9. Kang, D.H., T.S. Yun, K.Y. Kim, and J. Jang, *Effect of hydrate nucleation mechanisms and capillarity on permeability reduction in granular media.* Geophysical Research Letters, 2016. **43**(17): p. 9018-9025.

10. Jakobsen, M., J.A. Hudson, T.A. Minshull, and S.C. Singh, *Elastic properties of hydrate-bearing sediments using effective medium theory.* Journal of Geophysical Research: Solid Earth, 2000. **105**(B1): p. 561-577.

11. Lee, M.W. and T. Collett, *Elastic properties of gas hydrate-bearing sediments.* Geophysics, 2001. **66**(3): p. 763-771.

12. Sakai, A., *Can we estimate the amount of gas hydrates by seismic methods?* Annals of the New York Academy of Sciences, 2000. **912**: p. 374-391.

13. Santamarina, J.C., S. Dai, M. Terzariol, J. Jang, W.F. Waite, W.J. Winters, J. Nagao, J. Yoneda, Y. Konno, T. Fujii, and K. Suzuki, *Hydro-bio-geomechanical properties of hydrate-bearing sediments from Nankai Trough.* Marine and Petroleum Geology, 2015. **66**: p. 434-450.

14. Ta, X.H., T.S. Yun, B. Muhunthan, and T.-H. Kwon, *Observations of pore-scale growth patterns of carbon dioxide hydrate using X-ray computed microtomography.* Geochemistry, Geophysics, Geosystems, 2015. **16**(3): p. 912-924.

15. Kneafsey, T.J., Y. Seol, A. Gupta, and L. Tomutsa, *Permeability of laboratory-formed methane-hydrate-bearing sand: Measurements and observations using X-ray computed tomography.* SPE Journal, 2011. **SPE 139525**: p. 78-94.

16. Kunerth, D.C., D.M. Weinberg, J.W. Rector III, C.L. Scott, and J.T. Tohnson, *Acoustic laboratory measurements during the formation of a THF-hydrate in unconsolidated porous media*. Journal of Seismic Exploration, 2001. **9**: p. 337-354.

17. Kerkar, P., K.W. Jones, R. Kleinberg, W.B. Lindquist, S. Tomov, H. Feng, and D. Mahajan, *Direct observations of three dimensional growth of hydrates hosted in porous media*. Applied Physics Letters, 2009. **95**(2): p. 024102.

18. Schindler, M., M.L. Batzle, and M. Prasad, *Micro X-Ray computed tomography imaging and ultrasonic velocity measurements in tetrahydrofuran-hydrate-bearing sediments.* Geophysical Prospecting, 2016.

19. Dai, S. and Y. Seol, *Water permeability in hydrate-bearing sediments A pore-scale study*. Geophysical Research Letters, 2014. **41**: p. 4176-84.

20. Jung, J.W., J. Jang, J.C. Santamarina, C. Tsouris, T.J. Phelps, and C.J. Rawn, *Gas production from hydrate-bearing sediments: The role of fine particles.* Energy & Fuels, 2012. **26**: p. 480-7.

21. Minagawa, H., R. Ohmura, Y. Kamata, T. Ebinuma, H. Narita, and Y. Masuda. *Water permeability measurements of gas hydrate-bearing sediments*. in *The 5th International Conference on Gas Hydrates*. 2005. Trondheim, Norway.

22. Minagawa, H., Y. Sakamoto, T. Komai, and H. Narita. *Relation between pore-size distribution and permeability of sediment*. in *The 19th International Offshore and Polar Engineering Conference*. 2009. Osaka, Japan.

23. Minagawa, H., Y. Nishikawa, I. Ikeda, K. Miyazaki, N. Takahara, Y. Sakamoto, T. Komai, and H. Narita. *Measurement of water permeability and pore-size distribution of methane-hydrate-bearing sediments*. in *The 6th International Conference on Gas Hydrates*. 2008. Vancouver, Canada.

24. Minagawa, H., Y. Nishikawa, I. Ikeda, K. Miyazaki, N. Takahara, Y. Sakamoto, T. Komai, and H. Narita. *Relation between permeability and pore-size distribution of methane-hydrate-bearing sediments*. in *Offshore Technology Conference*. 2008. Houston, TX.

25. Chuvilin, E.M., T. Ebinuma, Y. Kamata, T. Uchida, S. Takeya, J. Nagao, and H. Narita, *Effects of temperature cycling on the phase transition of water in gas-saturated sediments.* Canadian Journal of Physics, 2003. **81**(1-2): p. 343-350.

26. Sakamoto, Y., T. Komai, Y. Kawabe, N. Tenma, and T. Yamaguchi, *Formation and dissociation behavior of methane hydrate in porous media - Estimation of permeability in methane hydrate reservoirs, Part 1* -. Journal of the Mining and Materials Processing Institute of Japan, 2004. **120**(2): p. 85-90.

27. Sakamoto, Y., T. Komai, Y. Kawabe, and T. Yamaguchi. *Properties of multiphase flow in marine sdeiments with gas hydrate*. in *5th ISOPE Ocean Mining Symposium*. 2003. Tsukuba, Japan.

28. Zheng, X. and J. Jang, *Hydraulic properties of porous media saturated with nanoparticle-stabilized air-water foam.* Sustainability, 2016. **8**(12): p. 1317.

29. ASTM, *C778-17 Standard specification for standard sand*. 2017.

30. Strauch, B., J.M. Schicks, M. Luzi-Helbing, R. Naumann, and M. Herbst, *The difference between aspired and acquired hydrate volumes – A laboratory study of THF hydrate formation in dependence on initial THF:H 2 O ratios.* The Journal of Chemical Thermodynamics, 2018. **117**: p. 193-204.

31. Sloan, E.D. and C.A. Koh, *Clathrate hydrates of natural gases*. 3rd ed. 2008, Boca Raton, FL: CRC Press, Taylor & Francis Group.

32. Yarveicy, H. and M.M. Ghiasi, *Modeling of gas hydrate phase equilibria: Extremely randomized trees and LSSVM approaches.* Journal of Molecular Liquids, 2017. **243**: p. 533-541.

33. Yarveicy, H., M.M. Ghiasi, and A.H. Mohammadi, *Determination of the gas hydrate formation limits to isenthalpic Joule–Thomson expansions.* Chemical Engineering Research and Design, 2018. **132**: p. 208-214.

34. Delli, M.L. and J.L.H. Grozic, *Experimental determination of permeability of porous media in the presence of gas hydrates.* Journal of Petroleum Science and Engineering, 2014. **120**: p. 1-9.

35. Masuda, Y., M. Kurihara, H. Ohuchi, and T. Sato. *A field-scale simulation study on gas productivity of formations containing gas hydrates*. in *Fourth International Conference on Gas Hydrates*. 2002. Yokohama, Japan.

36. Delli, M.L. and J.L.H. Grozic, *Prediction performance of permeability models in gas-hydrate-bearing sands.* SPE Journal, 2013. **18**(12): p. 274-284.

37. Chen, X., R. Verma, D.N. Espinoza, and M. Prodanović, *Pore-Scale Determination of Gas Relative Permeability in Hydrate-Bearing Sediments Using X-Ray Computed Micro-Tomography and Lattice Boltzmann Method.* Water Resources Research, 2018. **54**: p. 600-608.

38. Chen, X., R. Verma, D.N. Espinoza, and M. Prodanovic, *Pore-scale determination of gas relative permeability in hydrate-bearing sediments using X-ray computed micro-tomography and Lattice Boltzmann method*. Water Resources Research, 2018. **54**: p. 600-608.

39. Dvorkin, J., M.B. Helgerud, W.F. Waite, S.H. Kirby, and A. Nur, *Introduction to physical properties and elasticity models*, in *Natural Gas Hydrate*. 2000, Springer. p. 245-260.

40. Mavko, G., T. Mukerji, and J. Dvorkin, *The rock physics handbook: Tools for seismic analysis of porous media*. 2009: Cambridge university press.

41. Berryman, J.G., *Long-wavelength propagation in composite elastic media I. Spherical inclusions.* The Journal of the Acoustical Society of America, 1980. **68**(6): p. 1809-1819.

42. Yun, T.S., F.M. Francisca, J.C. Santamarina, and C. Ruppel, *Compressional and shear wave velocities in uncemented sediment containing gas hydrate.* Geophysical Research Letters, 2005. **32**(10): p. L10609.

43. Zheng, X., F. Perreault, and J. Jang, *Fines adsorption on nanoparticle-coated surface.* Acta Geotechnica, 2018. **13**: p. 219-226.

44. Mahabadi, N. and J. Jang, *The impact of fluid flow on force chains in granular media.* Applied Physics Letters, 2017. **110**(4): p. 041907.

45. Mahabadi, N., X. Zheng, T.S. Yun, L. van Paassen, and J. Jang, *Gas bubble migration and trappping in porous media: pore-scale simulation.* Journal of Geophysical Research - Solid Earth, 2018. **123**: p. 1060-1071.

46. Suh, H.S., D.H. Kang, J. Jang, K.Y. Kim, and T.S. Yun, *Capillary pressure at irregularly shaped pore throats: Implications for water retention characteristics.* Advances in Water Resources, 2017. **110**: p. 51-58.

47. Zheng, X., A.C. Barrios, F. Perreault, T.S. Yun, and J. Jang, *Interfacial tension and contact angle in CO2 -water/nanofluid-quartz system.* Greenhouse Gases: Science and Technology, 2018. **8**(4): p. 734-746.

48. Liu, W., Z. Wu, Y. Li, Y. Song, Z. Ling, J. Zhao, and Q. Lv, *Experimental study on the gas phase permeability of methane hydrate-bearing clayey sediments.* Journal of Natural Gas Science and Engineering, 2016. **36**: p. 378-384.

49. Gupta, A., *Methane hydrate dissociation measurements and modeling: the role of heat transfer and reaction kinetics*, in *Chemical Engineering Department*. 2007, Colorado School of MInes: Golden, CO.

50. Johnson, A., S. Patil, and A. Dandekar, *Experimental investigation of gas-water relative permeability for gas-hydrate-bearing sediments from the Mount Elbert Gas Hydrate Stratigraphic Test Well, Alaska North Slope.* Marine and Petroleum Geology, 2011. **28**(2): p. 419-426.

51. Minagawa, H., Y. Nishikawa, I. Ikeda, Y. Sakamoto, T. Komai, and H. Narita. *Measurement of methane hydrate sediment permeability using several chemical solutions as inhibitors*. in *The 7th ISOPE Ocean Mining Symposium*. 2007. Lisbon, Portugal.

52. Minagawa, H., K. Egawa, Y. Sakamoto, T. Komai, N. Tenma, and H. Narita. *Characterization of hydraulic permeability of methane-hydrate-bearing sediment estimated by T2-distribution of proton NMR*. in *The 22nd International Offshore and Polar Engineering Conference*. 2012. Rhodes, Greece.

53. Wang, J.-Q., J.-F. Zhao, M.-J. Yang, Y.-H. Li, W.-G. Liu, and Y.-C. Song, *Permeability of laboratory-formed porous media containing methane hydrate: Observations using X-ray computed tomography and simulations with pore network models.* Fuel, 2015. **145**: p. 170-179.

54. Liu, L., H. Zhang, C. Liu, C. Li, J. Sun, and Q. Meng, *Determining the permeaiblity of hydrate-bearing silty-fine sands with water transient flow*, in *CGS/SEG International Geophysical Conference*. 2017: Qingdao, China.

55. Chuvilin, E.M. and S.I. Grebenkin, *Gas permeability variations in gas-filled soils upon hydrate formation and freezing: An experimental study.* Scientific Journal Earth's Cryosphere, 2015. **XiX**(2): p. 59-64.

56. Berge, L.I., K.A. jacobsen, and A. Solstad, *Measured acoustic wave velocities of R11 (CCl3F) hydrate samples with and without sand as a function of hydrate concentration.* Journal of Geophysical Research, 1999. **104**(B7): p. 15415-15424.

57. Li, C.-H., Q. Zhao, H.-J. Xu, K. Feng, and X.-W. Liu, *Relation between relative permeability and hydrate saturation in Shenhu area, South China Sea.* Applied Geophysics, 2014. **11**(2): p. 207-214.

58. Priest, J.A., M. Druce, J. Roberts, P. Schultheiss, Y. Nakatsuka, and K. Suzuki, *PCATS Triaxial: A new geotechnical apparatus for characterizing pressure cores from the Nankai Trough, Japan.* Marine and Petroleum Geology, 2015. **66**: p. 460-470.

59. Konno, Y., J. Yoneda, K. Egawa, T. Ito, Y. Jin, M. Kida, K. Suzuki, T. Fujii, and J. Nagao, *Permeability of sediment cores from methane hydrate deposit in the Eastern Nankai Trough.* Marine and Petroleum Geology, 2015. **66**: p. 487-495.

60. Yoneda, J., A. Masui, Y. Konno, Y. Jin, K. Egawa, M. Kida, T. Ito, J. Nagao, and N. Tenma, *Mechanical properties of hydrate-bearing turbidite reservoir in the first gas production test site of the Eastern Nankai Trough.* Marine and Petroleum Geology, 2015. **66**: p. 471-486.

61. Lee, M.W., *Models for gas hydrate-bearing sediments inferred from hydrate permeability and elastic velocities.* 2008, U.S. Geological Survey.

62. Kleinberg, R.L., C. Flaum, and T.S. Collett, *Magnetic resonance log of JAPEX.JNOC:GSC et al. Mallike 5L-38 gas hydrate produciton research well: gas hydrate saturation, growth habit, and relative permeability*, in *cientific Results from the Mallik 2002 Gas Hydrate Production Research Well Program, Mackenzie Delta, Northwest Territories, Canada*, S.R. Dallimore and T.S. Collett, Editors. 2005, Geological Survey of Canada.

63. Murray, D., M. Fukuhara, C.K. Khong, T. Namikawa, and K. Yamamoto, *Permeability estimates in gas hydrate reservoirs of the Nankai Trough*, in *SPWLA 47th Annual Logging Symposium*. 2006: Veracruz, Mexico.

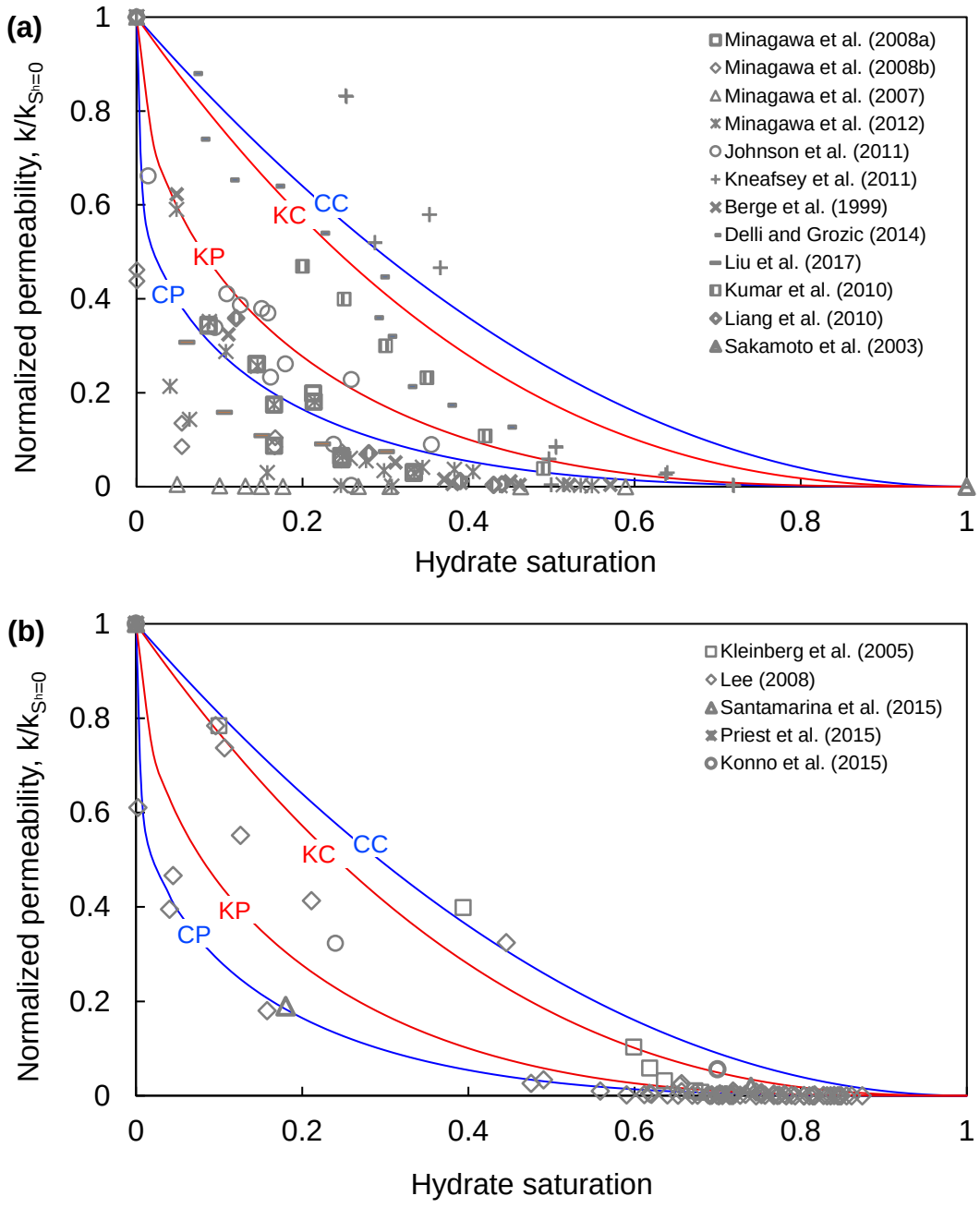

Figure 1. Water permeability as a function of hydrate saturation – a compilation of published experimental data with reference to analytical models. (a) Water permeability of laboratory-formed hydrate-bearing sediments. (b) Water permeability of the pressure cores of the natural hydrate-bearing sediments (never experienced depressurization). The results of the analytical models (capillary tube model-coating CC, capillary tube model-pore-filling CP, Kozeny grain model-coating KC, and Kozeny grain model-pore filling KP) are superimposed.

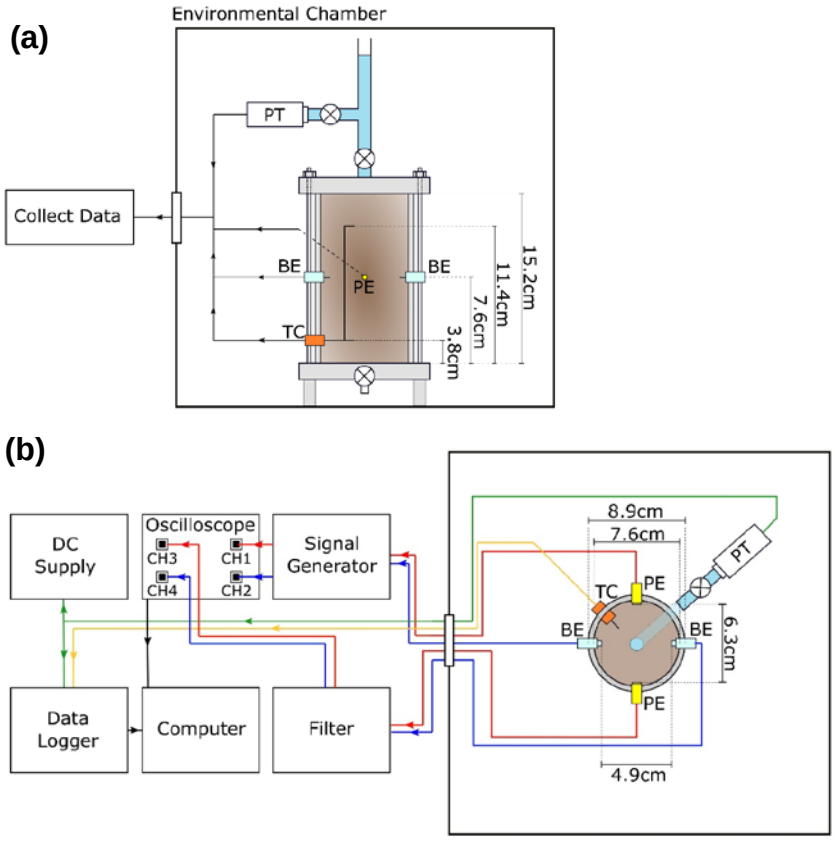

Figure 2. Illustrations of the experimental setup. (a) Test configuration for measurement of permeability and wave velocity, with the installed components: pressure transducer PT, bender element BE, piezo-crystal PE, and thermocouple TC. (b) Connection details for P- and S-wave measurement.

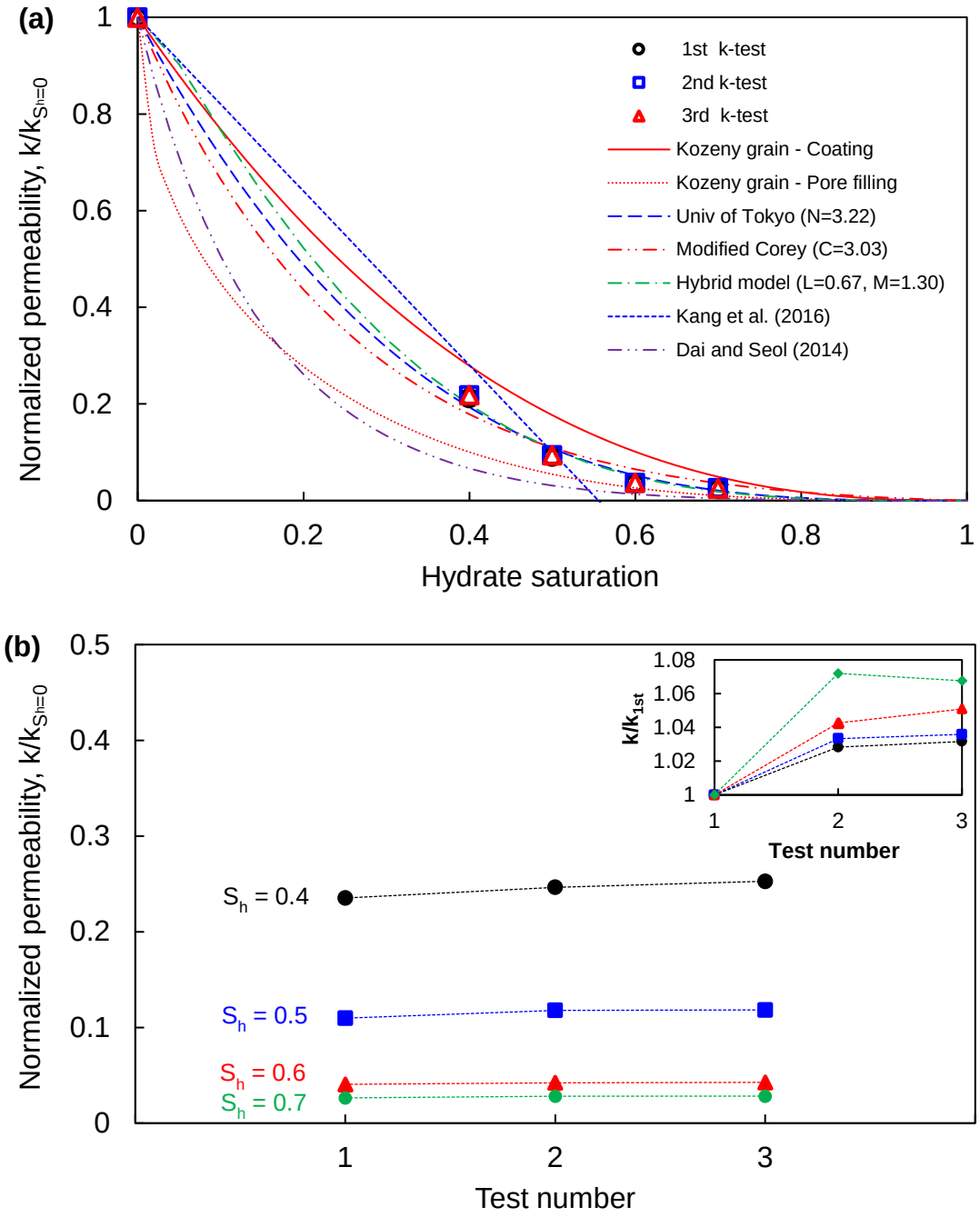

Figure 3. Measured permeability in THF hydrate-bearing sediments. (a) Normalized water permeability as a function of hydrate saturation. Three permeability values at a given hydrate saturation are shown (The measured permeability of hydrate-free sediment is 81.1mD). (b) Normalized water permeability measured three different times for a given THF hydrate-bearing sediments.

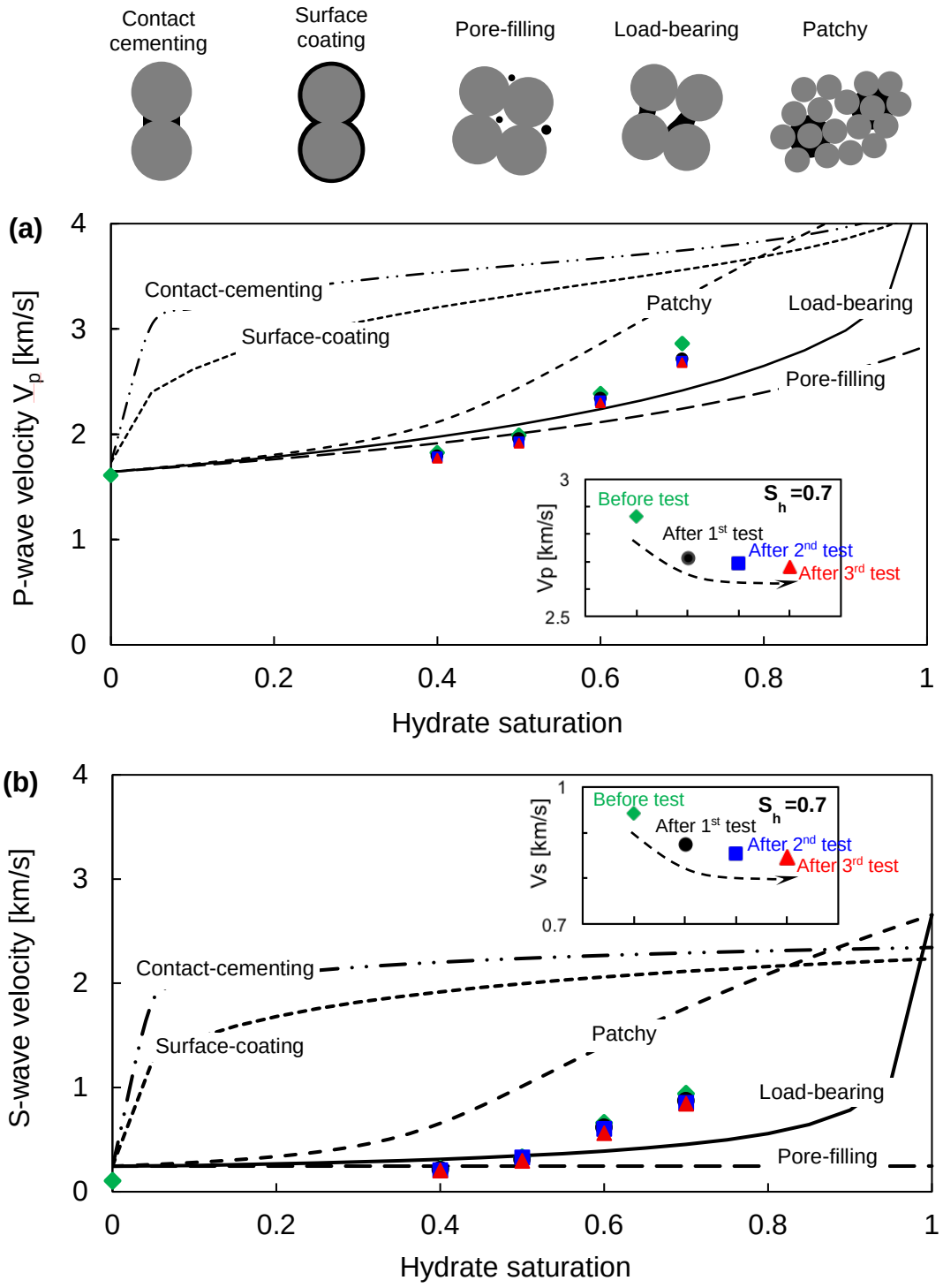

Figure 4. Compressional (P-) and shear (S-) wave velocity measurements before and after permeability test. (a) Compressional and (b) shear wave velocities. P- and S-wave velocities are measured right after every hydraulic conductivity test. Note that the schematic hydrate configurations in the pore space are drawn for the four different pore habits.

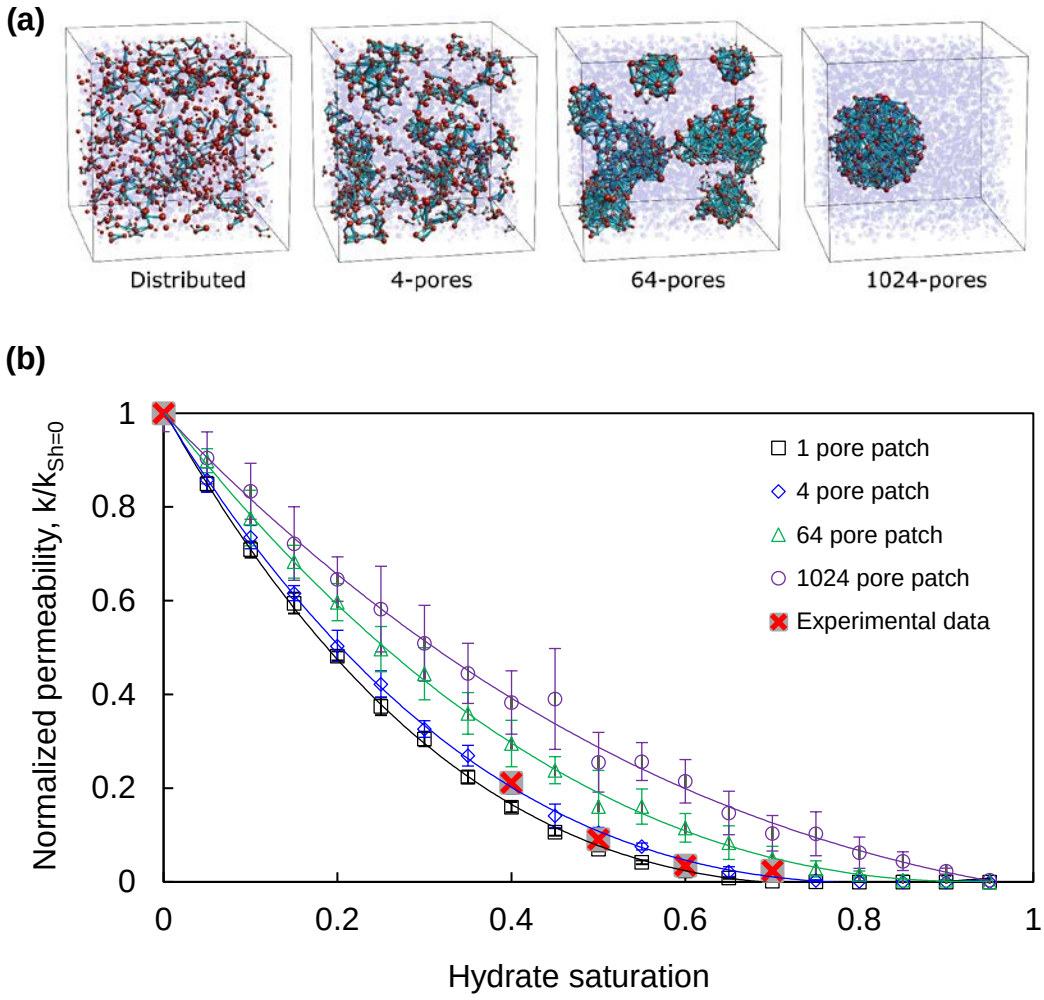

Figure 5. Numerical results of water permeability in hydrate-bearing sediments. (a) Various types of hydrate patch for a given hydrate saturation S_h=0.2 in the pore network model: distributed, 4-pore, 64-pore, and 1024-pore. For a hydrate saturation of higher than 50%, a few of the generated hydrate patches are interconnected even for the 4- or 64-pore patches. The pore-network model consists of 4593 pores and 19361 tubes with a mean tube connectivity per pore (coordination number) of cn=6.8. Mean pore radius is μ[R_{pore}]=69 μm, mean tube size is μ[R_{tube}]=12 μm, and mean tube length is μ[L_{tube}]=45 μm (max[R_{pore}]=194 μm, min[R_{pore}]=22 μm, max[R_{tube}]=63 μm, min[R_{tube}]=1 μm, max[L_{tube}]=201 μm, min[L_{tube}]=0.06 μm). (b) The effect of the hydrate pore habit on permeability reduction trend – A pore-network model simulation. As the size of the hydrate patch (the number of pores forming one cluster of hydrates) increases, the permeability increases for a given hydrate saturation.